RSC Advances

PAPER

View Article Online
View Journal | View Issue



Cite this: *RSC Adv.*, 2022, **12**, 14260

# $Ti_3C_2$ MXene-anchored photoelectrochemical detection of exosomes by *in situ* fabrication of CdS nanoparticles with enzyme-assisted hybridization chain reaction†

Zhenli Qiu, ‡[ab] Dechun Fan,‡[ac] XiangHang Xue,[a] Jiayi Zhang,[a] Jiaolin Xu,[a] Haixia Lyu *[c] and Yiting Chen*[ad]

Exosomes that carry large amounts of tumor-specific molecular information have been identified as a potential non-invasive biomarker for early warning of cancer. In this work, we reported an enzyme-assisted photoelectrochemical (PEC) biosensor for quantification of exosomes based on the *in situ* synthesis of $Ti_3C_2$ MXene/CdS composites with magnetic separation technology and hybridization chain reaction (HCR). First, exosomes were specifically bound between aptamer-labeled magnetic beads (CD63-MBs) and a cholesterol-labeled DNA anchor. The properly designed anchor ends acted as a trigger to enrich the alkaline phosphatase (ALP) through HCR. It catalyzed more sodium thiophosphate to generate the sulfideion ($S^{2-}$), which combined with $Cd^{2+}$ for *in situ* fabrication of CdS on $Ti_3C_2$ MXene resulting in elevated photocurrent. The $Ti_3C_2$ MXene-anchored PEC method was realized for the quantitative detection of exosomes, which exhibited the dynamic working range from $7.3 \times 10^5$ particles per mL to $3.285 \times 10^8$ particles per mL with a limit of detection of $7.875 \times 10^4$ particles per mL. The strategy showed acceptable stability, high sensitivity, rapid response and excellent selectivity. Furthermore, we believe that the PEC biosensor has huge potential as a routine bioassay method for the precise quantification of exosomes from breast cancer in the future.

Received 9th March 2022
Accepted 20th April 2022

DOI: 10.1039/d2ra01545e

rsc.li/rsc-advances



## Introduction

Exosomes are a small homogeneous (50–150 nm) subgroup of membrane vesicles originating from late endosomes and secretions, which carry tumor-specific biomolecules, including lipids, proteins, and nucleic acids.[1,2] Besides, exosomes are secreted by all types of cells and can be detected in a variety of body fluids, including blood, breast milk, tears, urine, amniotic fluid and saliva.[3,4] The body fluid samples are easy to obtain, and most body fluids are sampled without causing any damage to the body. Therefore, exosomes are widely recognized as a potential non-invasive biomarker for bioanalytical applications, cancer surveillance and disease therapeutics.[5] Currently, increasingly new technologies have been proposed to improve the sensitivity of exosomes, including surface enhanced Raman scattering (SERS),[6] electrochemistry,[7] nanoplasmonic sensors,[8] localized surface plasmon resonance (LSPR),[9] colorimetry[10] and so on. However, some analytical techniques for exosome quantification relies on expensive and specialized instruments with the expertise to operate. Therefore, it is urgent to develop novel, highly sensitive and reliable diagnostic techniques for tumor exosomes detection in the clinical research.

Compared with other methods, the PEC biosensor with higher sensitivity and lower background signal provides an emerging approach,[11,12] which is based on the photo-generated electron transfer between the solution and the electrode surface under the irradiation of light.[13,14] Seeking high performance materials is an effective means to break through the bottleneck of PEC biosensor. Two-dimensional nanomaterials, transition metal carbides/carbonitrides (MXenes), have attracted tremendous attention to areas of importance in recent years due to their ultrathin structure and excellent physiochemical properties. As has been reported,[15–17] MXenes are synthesized by extracting a kind of element A from the layered ternary carbides of MAX phase, where M stand for an early transition metal (V,

[a]*College of Materials and Chemical Engineering, Minjiang University, Fuzhou 350108, China. E-mail: cyt@mju.edu.cn*

[b]*Fujian Engineering and Research Center of New Chinese Lacquer Materials, Fuzhou 350108, China*

[c]*College of Materials Science and Engineering, Fuzhou University, Fuzhou, 350108, China*

[d]*Fujian Provincial University Engineering Research Center of Green Materials and Chemical Engineering, Fuzhou 350108, China*

† Electronic supplementary information (ESI) available: Experimental details; FT-IR spectrum; UV-vis absorption spectrum. See https://doi.org/10.1039/d2ra01545e

‡ These authors contributed equally to this work.

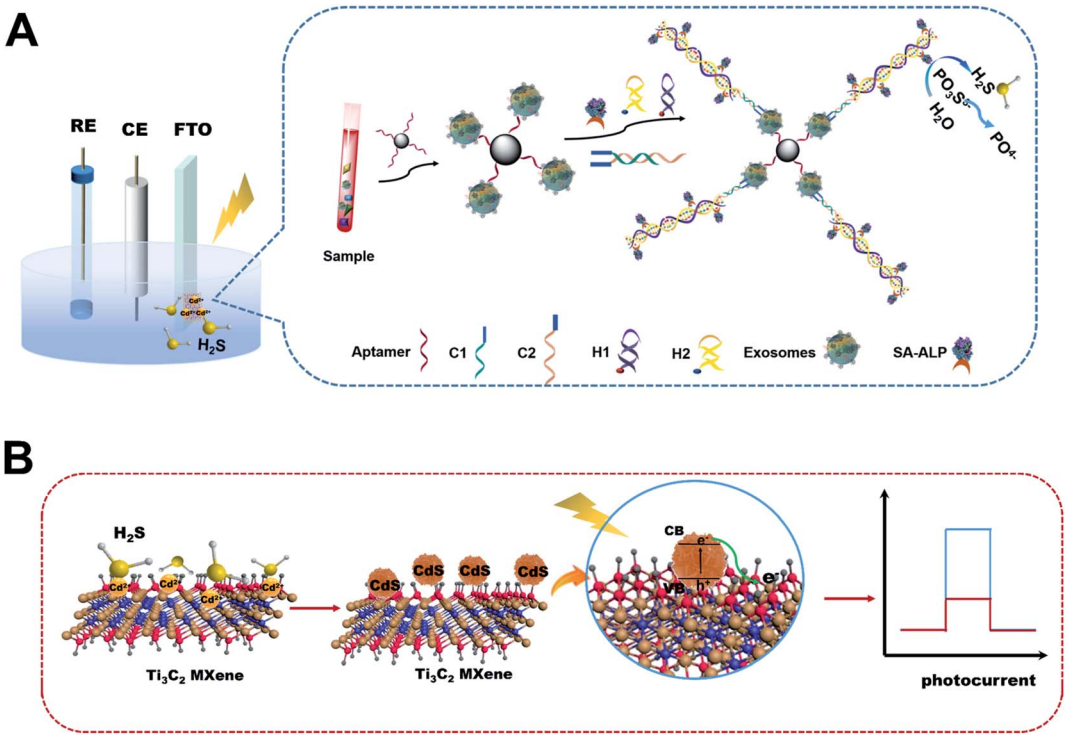


Scheme 1 (A) Schematic Illustration of $Ti_3C_2$ MXene-anchored photoelectrochemical detection of exosomes by *in situ* fabrication of CdS nanoparticles with enzyme-assisted hybridization chain reaction and (B) the possible charge transfer mechanism for the *in situ* fabrication of $Ti_3C_2$ MXene/CdS.

Cr, Nb, Mo, Mn, Sc, Ti, Zr, Hf, Ta), A is a member from 12–16 A-group element (S, P, As, Pb, Ti, Cd, In, Sn, Ge, Ga, Si, Al), and X is either C or N. MXene not only has metal-like electrical conductivity, but also has excellent chemical reactivity and hydrophilicity due to its abundant functional groups such as –F and –OH on its surface, which is expected to be an ideal matrix material for the construction of nanocomposite structures. However, due to the exposure of a high proportion of metal atoms on the surface, MXene is easily oxidized and accompanied by the collapse of two-dimensional structure. A great deal of efforts has been made to enhance the interfacial interactions between $Ti_3C_2Tx$ layers, for example, by incorporating polymers or metal ions into $Ti_3C_2T_x$ as reinforcement fillers. Li *et al.* reported an effective ion sieving with $Al^{3+}$-intercalated MXene membranes for seawater desalination.[18] Wu *et al.* prepared hierarchical $MoS_2/Ti_3C_2$-MXene@C nanohybrids with excellent performance of Li storage and hydrogen evolution reaction, which efficiently stabilized the structure of $Ti_3C_2$-MXene and prevented its spontaneous oxidation.[19]

In this work, we took advantage of an enzyme-assisted amplification strategy by hybridization chain reaction to develop the $Ti_3C_2$ MXene-anchored PEC biosensor for the detection of exosomes from breast cancer (Scheme 1). The acquisition of enhanced photocurrent signals was derived from the *in situ* synthesis of CdS nanoparticles on $Ti_3C_2$ MXene-modified electrode through the exosomes-initiated DNA cascades. As shown in Scheme 1, a considerable amount of exosomes was specifically captured by the CD63-MBs. Then, the exosome membrane inserted the cholesterol-labeled DNA probe (C1 and C2) and the base sequence from the 5′ end of C2 probe triggered a hybridization chain reaction. Meanwhile, introduction of streptavidin-labeled ALP interacted with the biotin labeled DNA probe (H1 and H2). The ALP catalyzed the *p*-nitrophenyl phosphate to sulfideion and inorganic phosphate in the presence of thioglycerol. CdS are generated *in situ* on $Ti_3C_2$ MXenes by 1-thioglycerol as a protective agent. The *in situ* synthesis of CdS nanoparticles on $Ti_3C_2$ MXene could effectively inhibit the oxidation of MXene and improve the structural stability due to its physical barrier and limited effect. Furthermore, the Fermi energy level of the two-dimensional $Ti_3C_2$ MXene layer could match the band gap energy of CdS, and it is beneficial to the separation and transmission of photo-carriers. The difference between the valence band of CdS and the Fermi level of $Ti_3C_2$ MXene led to the formation of a built-in electric field at the interface, which reduced the recombination of electron–hole pairs and increased the PEC signal. Therefore, the concentration of exosomes was a direct reflection of the photocurrent changes from the *in situ* growth of $Ti_3C_2$ MXene/CdS composites, which could be explored for the sensitive detection of low abundance exosomes in breast cancer.

## Results and discussion

### Characterization of $Ti_3C_2$ MXene/CdS composites

The morphology and microstructures of $Ti_3C_2$ MXene, CdS and $Ti_3C_2$ MXene/CdS composites were observed by scanning

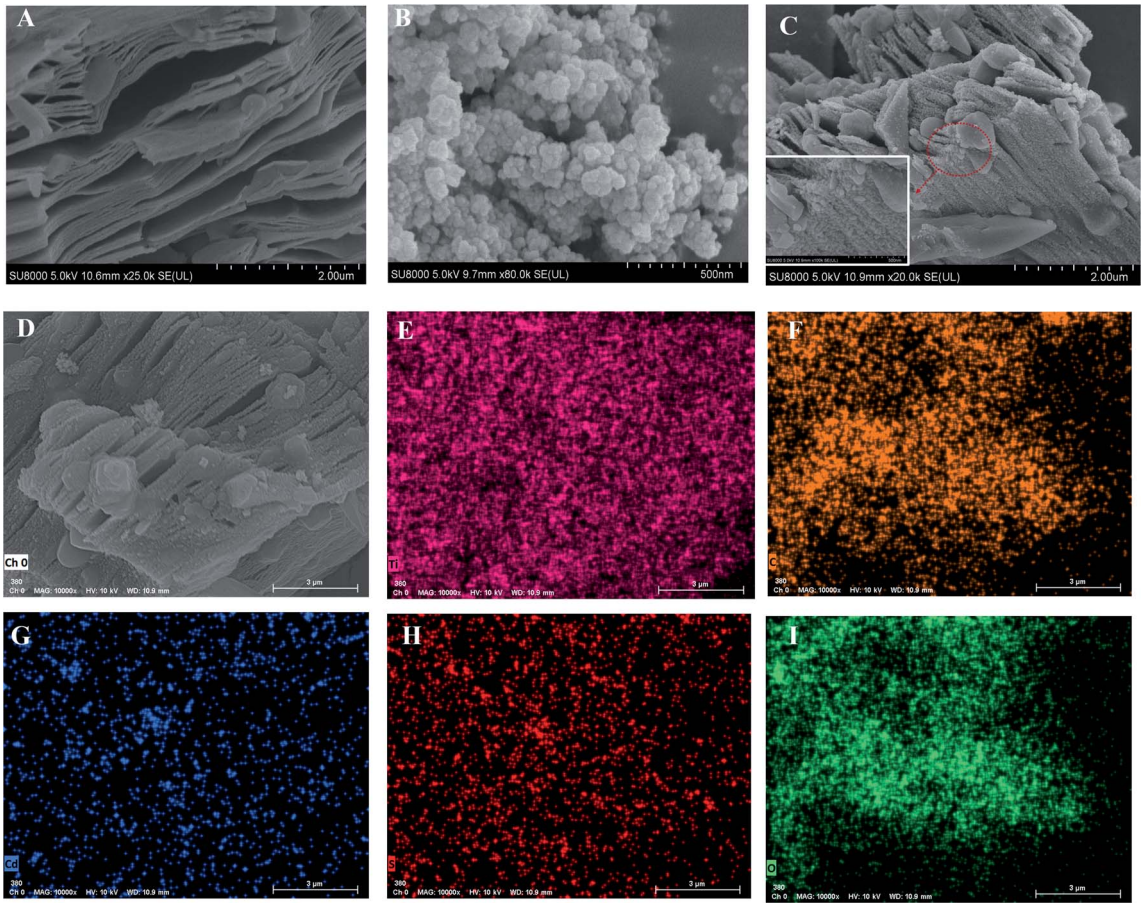


Fig. 1 SEM image of (A) $Ti_3C_2$ MXene, (B) CdS, (C) $Ti_3C_2$ MXene/CdS. (D–I) The corresponding elemental mapping images of Ti, C, Cd, S and O in $Ti_3C_2$ MXene/CdS, respectively.

electron microscopy (SEM, Hitachi, SU8010, Japan). Fig. 1A showed the organ-like structure of $Ti_3C_2$ MXene after HF corrosion, and the thickness of each layer was about tens of nanometers. As shown in Fig. 1B, we could see clearly that the CdS was granular with diameter of 80∼120 nm. From the image of $Ti_3C_2$ MXene/CdS composites (Fig. 1C), CdS nanoparticles were embedded in the clearance between layers of the organ-like structure of $Ti_3C_2$ MXene. Moreover, elemental mapping was also performed to further confirm the composition and distribution in $Ti_3C_2$ MXene/CdS composites. Ti-, C-, Cd-, S- and O-based mappings of $Ti_3C_2$ MXene/CdS composites were presented in Fig. 1D–I, revealing that the CdS was uniformly distributed on the surface of $Ti_3C_2$ MXene. SEM images proved that the exosomes-triggered HCR signal amplification could successfully generate CdS *in situ* on the surface of $Ti_3C_2$ MXene.

To investigate the phase structure of $Ti_3C_2$ MXene, CdS and $Ti_3C_2$ MXene/CdS composites, X-ray diffraction (XRD, Rigaku, Miniflex, Japan) was used to characterize the samples. As shown in Fig. 2A, we obtained the XRD pattern of amorphous pure CdS (curve a) catalyzed by ALP, and the diffraction peaks appearing at 26.94°, 44.26°, and 52.04° were indexed to the (111), (220), and (311).[20] Also, the peaks intensities of pure $Ti_3C_2$ (curve b) at 8.70° 18.24°, 28.12°, and 60.94° corresponded to the (002), (004), (006), (110) crystal plane of $Ti_3C_2$ MXene,[21] indicating that the $Ti_3C_2$ MXene was successfully fabricated. With the *in situ* fabrication of CdS nanoparticles on $Ti_3C_2$ MXene (curve c), the diffraction peak signals of $Ti_3C_2$ MXene declined significantly, while the peaks of CdS enhanced gradually. The diffraction peak of $Ti_3C_2$/CdS composites (curve c) existed at both 8.70°, 60.94° and 26.94° matched with $Ti_3C_2$ MXene and CdS respectively, and other diffraction peaks of $Ti_3C_2$ MXene/CdS composites overlapped with those of CdS and $Ti_3C_2$ MXene. This could be interpreted as the fact that CdS generated *in situ* on the surface of $Ti_3C_2$ MXene. The X-ray photoelectron spectrum (XPS, Thermo Fisher Scientific, Verios G 4UC, USA) was used to further investigate the elements of the $Ti_3C_2$ MXene/CdS composites on the electrode surface, and accurately measure the internal electron binding energy and chemical states of an atom. As see from Fig. 2B, the survey spectrum of $Ti_3C_2$ MXene/CdS composites consisted of predominant elements, including Ti, C, O, Cd, F and S. In addition, the charge of F element could be attributed to the residual HF in the etching process.[22] Fig. 2C shows that a high-resolution XPS spectrum of Cd 3d 411.92 eV and 405.17 eV belonged to Cd $3d_{3/2}$ and Cd $3d_{5/2}$, respectively. For the S 2p XPS spectra (Fig. 2C, inset), the binding energy of S $2p_{1/2}$ and S $2p_{2/3}$ located at 162.75 eV and 161.51 eV,

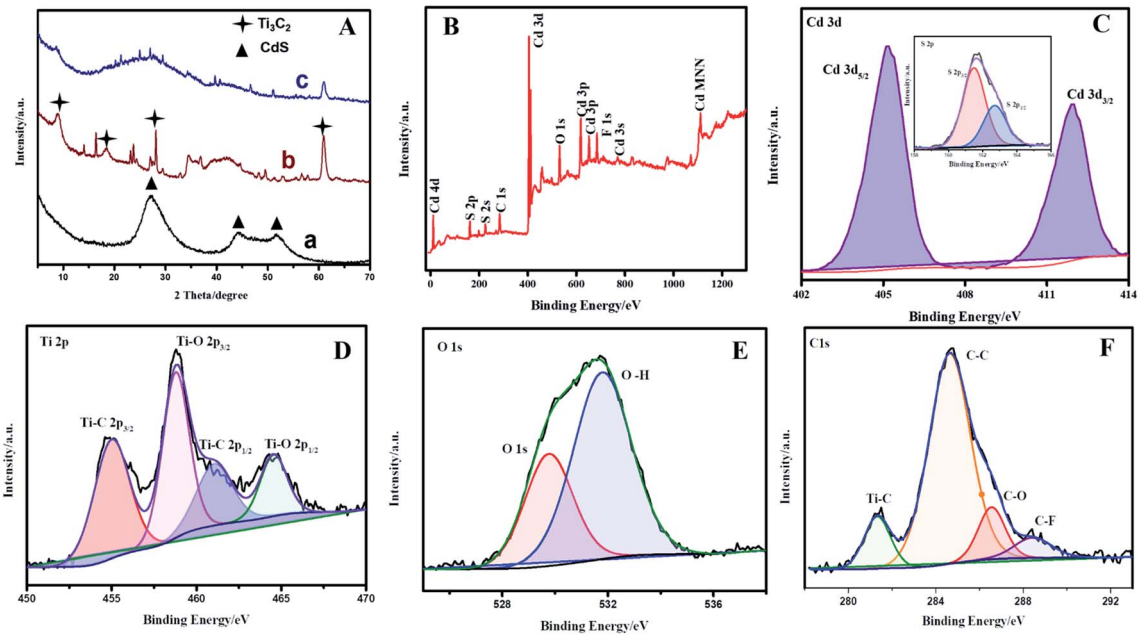


Fig. 2 (A) XRD patterns of (a) CdS, (b) $Ti_3C_2$ MXene and (c) $Ti_3C_2$ MXene/CdS. (B) X-ray photoelectron spectroscopy (XPS) survey spectrum of $Ti_3C_2$ MXene/CdS composites. High-resolution XPS spectra for (C) Cd 3d (insert: S 2p), (D) Ti 2p, (E) O 1s and (F) C 1s of $Ti_3C_2$ MXene/CdS composites.

respectively. As shown in Fig. 2D, the two peaks of Ti 2p located at 461.14 eV and 455.01 eV, which were attributed to the Ti–C bond.[22–24] While the other two peaks at 464.54 eV and 458.85 eV were assigned to the Ti–O bond.[25] The O 1s peaks at approximately 529.4 eV and 531.8 eV (Fig. 2E) might be derived from the bonds of Ti–O–Ti and O–H, respectively.[26] Furthermore, C 1s could be divided into four characteristic peaks, which located at 281.29 eV, 284.61 eV, 286.54 eV, and 288.43 eV, corresponding chemical bonds with C–Ti, C–C/C–H, C–O, and C–F (Fig. 2F).[23] All of the above results further confirmed that CdS formed *in situ* in the interlayer space of $Ti_3C_2$ MXene.

### Feasibility of $Ti_3C_2$ MXene-anchored PEC biosensor

In order to further verify the aptamer had been successfully modified to the surface of MBs, the FT-IR spectrum (Thermo Fisher Scientific, Nicolet iS5, USA) of carboxy-modified magnetic beads (curve a) and CD63-modified MBs (curve b) were measured in Fig. S1A.† The CD63 modified-MBs showed the characteristic peaks of methylene asymmetrical C–H stretching (2974 $cm^{-1}$), C=O stretching vibration (1653 $cm^{-1}$), N–H bending vibration (1568 $cm^{-1}$), –OH bending vibration (1319 $cm^{-1}$) and C=O stretching (1080 $cm^{-1}$), which demonstrated that CD63 had successfully coated amide bond with MBs.[27,28] As shown in Fig. S1B,† UV-visible (UV-vis) absorption spectrum (Hitachi, U-3900, Japan) were used to monitor the conjugate of MBs-CD63 aptamer (curve a), there was a distinct peak at 269 nm, while the absorption of MBs (curve b) was absent in this region. Obviously, the absorption at 269 nm could be attributed to the characteristic absorption of the CD63 aptamer.[29] These results verified that the aptamer was grafted to the MBs.

To investigate the feasibility of the $Ti_3C_2$ MXene-anchored PEC biosensor for the detection of exosomes, exosomes were extracted from supernatant of MCF-7 cells. The morphology of exosome samples was observed by transmission electron microscope (TEM, HITACHI, HT7800, Japan). Fig. 3A displayed that typical saucer-like exosome particles and had good structural integrity with an average diameter of about 130 nm, whose size and morphology are consistent with previous reports.[30] In addition, the concentration of isolated exosomes was analyzed by nanoparticle tracking analysis (NTA) as showed in Fig. S2.† The average particle size was about 127 nm, which was consistent with the typical size of exosomes (50–150 nm) and TEM image. Western blot method was used to analyze the effective exosome-specific surface proteins CD81 and TSG101. As shown in Fig. 3B, the test results of CD81 and TSG101 label proteins from the extracted exosomes were both positive by western blot analysis, indicating that the extracted samples were exosomes from MCF-7 cells. These results together confirmed that exosomes had been successfully extracted from MCF-7 cells, so these isolated exosomes could be used for subsequent validation experiments.

In order to confirm the success of the hybrid chain reaction, polypropylene gel electrophoresis (PAGE) analysis was performed in Fig. 3C. Bands 1–4 clearly referred to the DNA sample of C1, C2, H1 and H2, respectively. Lane 5 (C1 + C2) demonstrated the emergence of a new band (about 80 bp), indicating that a hybrid double strand could be formed by mixing C1 and C2. When the bands H1 and H2 were mixed, only a band with an equal base number of H1 and H2 were found, indicating that the two kind of DNA coexisted stably without hybridization chain reaction (Lane 6). When C1 was incubated with H1 and

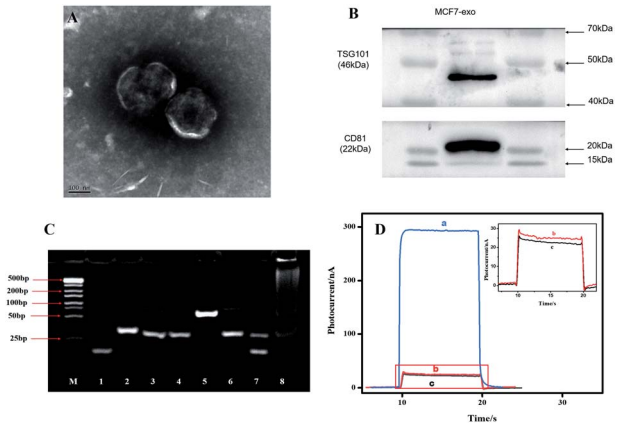


Fig. 3 (A) TEM image of exosomes, (B) Western blotting images of TSG101 and CD81 proteins in the exosomes form MCF-7 cells. (C) PAGE image of HCR assay. Lane M, 25–500 bp DNA marker; Lane 1, C1; Lane 2, C2; Lane 3, H1; Lane 4, H2; Lane 5, C1 + C2; Lane 6, H1 + H2; Lane 7, C1 + H1 + H2; and Lane 8, C1 + C2 + H1 + H2. (D) Photocurrent responses of $Ti_3C_2$ MXene/$Cd^{2+}$/FTO electrode in the (b) absence and (a) presence of $1.825 \times 10^8$ particles per mL exosomes compared with background signal of (c) $Ti_3C_2$ MXene/FTO.

H2, the bands similar to Lane 1 (C1) and Lane 6 (H1 + H2) could be seen in Lane 7, demonstrating that C1 could not open the hairpin structure of H1 to form the hybridization chain reaction. Compared with Lane 7, the incubation of C1, H1 with H2 in the presence of C2, a single obvious HCR band appeared (Lane 8). These results suggested that the HCR strategy could be implemented easily in the presence of C1, H1 and H2 with the assistance of C2.

Logically, a question arises as to whether the target-triggered HCR strategy could *in situ* generate $Ti_3C_2$ MXene/CdS composites that cause photocurrent changes for the detection of exosomes. Therefore, we investigated the feasibility of the $Ti_3C_2$ MXene-anchored PEC biosensor by tracking the photocurrent variation of the photo-electrode at different stages (Fig. 3D). The $Ti_3C_2$ MXene-modified photo-electrode obtained a relatively weak photocurrent, suggesting that $Ti_3C_2$ MXene-anchored PEC biosensor had a low background signal (curve 'c'). As a non-specific adsorption control test, the photocurrent response was almost the same as the curve 'a' in the absence of the target (curve 'b'), which indicated that the non-specific adsorption had little influence on this PEC system. When the $S^{2-}$ generated from enzyme-catalyzed reaction based on HCR to *in situ* fabrication of CdS on $Ti_3C_2$ MXene in the presence of $1.825 \times 10^8$ particles per mL exosomes (curve 'a'), the photocurrent had obviously improved compared to the $Ti_3C_2$ MXene-modified photoelectrode (curve 'c'). The results were attributed to more efficient transport and better charge carrier separation in the *in situ* fabrication of $Ti_3C_2$ MXene/CdS composites.

## Optimization of PEC measurement conditions

In this work, to improve the excellent performance of exosome detection, we optimized several conditions, such as $Cd^{2+}$ concentration, sodium thiophosphate (TP) concentration, 1-thioglycerol (TG) concentration and enzyme-catalyzed reaction time by HCR strategy in the test solution.

First, the concentration of sodium thiophosphate (TP) was optimized from 1 to 10 mM as the substrate for enzyme catalysis (Fig. 4A). The maximum photocurrent was obtained when the TP concentration reached 8.0 mM, and then decreased with the increase of TP concentration, which might be attributed to the excessive deposition of sodium thiophosphate on the electrode, resulting in inhibition of electron and proton transport. Another key factor affecting photocurrent response was the concentration of 1-thioglycerol (TG). The effects of 1-thioglycerol concentration were investigated to evaluate the optimal response of $Ti_3C_2$ MXene-anchored PEC system (Fig. 4B). The photocurrent increased sharply with the increase of TG concentration from 0 to 0.7 M. In the presence of 0.7 M TG solution, the photocurrent response value reached the plateau stage, so this concentration of TG (0.7 M) was selected in the follow-up experiments. TG severed as ligands of *in situ* CdS nanoparticles and significantly improved the redox reaction on the electrode surface.[31] Therefore, the concentration of TG and TP was 0.7 M and 8 mM for enzyme-catalyzed reaction, respectively. In addition, the concentration of $Cd^{2+}$ ions had a significant meaning in the *in situ* generation of CdS nanoparticles on $Ti_3C_2$ MXene-modified photo-electrode. The low abundance of $Cd^{2+}$ might limit the detection range of this proposed PEC sensing platform, and the high-abundant $Cd^{2+}$ ions might hinder electron transport. As shown in Fig. 4C, when the concentration of $Cd^{2+}$ was 0.2 M, the photocurrent reached its maximum value. Therefore, 0.2 M $Cd^{2+}$ was used in the *in situ* formation process of CdS nanoparticles.

Finally, the influence of the enzyme-catalyzed reaction time for sodium thiophosphate by HCR on the photocurrent was monitored (Fig. 4D). The photocurrent increased with increasing incubation time and the platform was observed at 90 minutes, demonstrating that the whole reaction time reached

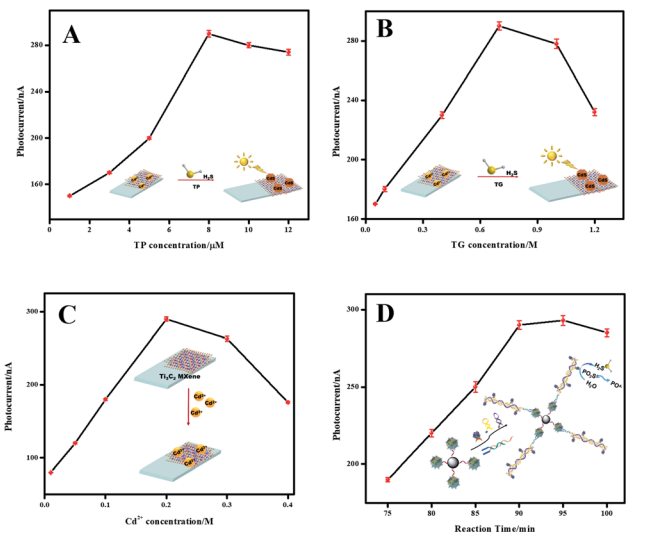


Fig. 4 Effects of (A) TP concentration, (B) TG concentration, (C) $Cd^{2+}$ ions concentration and (D) reaction time on the PEC photocurrent response obtained in the test solution.

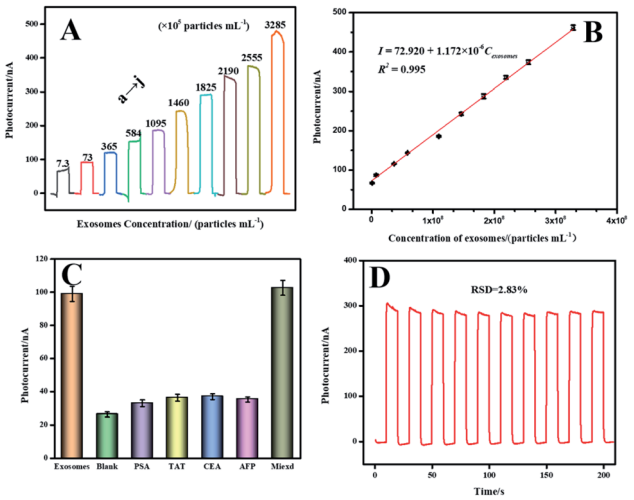


Fig. 5 (A) Photocurrent response toward the different concentrations of exosomes: (a) 7.3 × $10^5$ particles per mL, (b) 7.3 ×$10^6$ particles per mL, (c) 3.65 × $10^7$ particles per mL, (d) 5.84 × $10^7$ particles per mL, (e) 1.095 × $10^8$ particles per mL, (f) 1.460 × $10^8$ particles per mL, (g) 1.825 × $10^8$ particles per mL, (h) 2.190 × $10^8$ particles per mL, (i) 2.555 × $10^8$ particles per mL, (j) 3.285 × $10^8$ particles per mL. (B) Corresponding calibration curve of biosensor platform. (C) The specificity of PEC biosensors for exosomes (7.3 ×$10^6$ particles per $mL^{-1}$) compared with interferences including CEA (100 ng $mL^{-1}$), AFP (100 ng $mL^{-1}$), PSA (100 ng $mL^{-1}$), TAT (100 ng $mL^{-1}$). (D) The stability of the PEC biosensor towards 1.825 × $10^8$ particles per mL exosomes.

equilibrium. Considering the above experimental results, 0.8 mM TP, 0.7 M TG, 0.2 M $Cd^{2+}$ and the enzyme-catalyzed reaction time by HCR of 90 min were applied to the subsequent experiments.

### Quantitative analysis of exosomes *via* PEC biosensor

Taking advantage of the above optimal experimental conditions, we further evaluated the performance of our PEC method for quantitative detection of exosomes at different concentrations. Fig. 5A illustrated that an increase in photocurrent intensity with the increase of the exosome concentration from breast cancer. Furthermore, a plot of the photocurrent response against the concentration of exosomes showed a good linear relationship within the detection range of 7.3 × $10^5$ particles per mL–3.285 × $10^8$ particles per mL (Fig. 5B). The corresponding equation correlation equation was $\Delta I = 72.920 + 1.172 \times 10^{-6} C_{exosomes}$ ($R^2$ = 0.995). The limit of detection (LOD) of $Ti_3C_2$ MXene-anchored PEC biosensor was calculated as 7.875 × $10^4$ particles per mL, based on $3\sigma/k$ ($\sigma$ and $k$ represent the standard deviation of the blank sample and the slope of the equation, respectively).

### The stability, reproducibility and selectivity of the constructed PEC system

In view of practical application, it was of great significance to test the stability, reproducibility and selectivity of $Ti_3C_2$ MXene-anchored PEC biosensor. Our proposed PEC approach for exosome detection mainly relied on the specific recognition between aptamer and exosome. To further investigate the selectivity of this PEC biosensor, we used different types of cancer biomarkers in human serum for PEC sensing analysis, *e.g.* carcinoembryonic antigen (CEA), prostate-specific antigen (PSA), alpha-fetoprotein (AFP), thrombin-antithrombin complex (TAT). As displayed in Fig. 5C, the photocurrent signal generated by exosomes (7.3 ×$10^6$ particles per mL) was significantly higher than other interferers. And the photocurrent response of other interferers was similar to the background signal. Furthermore, in the presence of 7.3 ×$10^6$ particles per mL exosomes and interfering substance, the photocurrent values were similar to those in the presence of 7.3 ×$10^6$ particles per mL exosomes alone. The result revealed that the interferences had little effect on the detection of exosomes and provided sufficient possibilities for selective detection of exosomes.

The stability of the as-prepared $Ti_3C_2$ MXene/$Cd^{2+}$/FTO photoelectrode was monitored by assaying 1.825 × $10^8$ particles per mL exosomes standard sample. As shown in Fig. 5D, the photocurrent was basically stable and conformed to high stability through the automatic control of "on–off" light irradiation (10 times). The photocurrent response with 10 cycles was recorded with a relative standard deviation of 2.83%. The interaction between $Cd^{2+}$ and oxygen-containing functional groups on the surface of MXene nanosheets could fix the layer spacing. The *in situ* synthesis of CdS nanoparticles on $Ti_3C_2$ MXene could effectively inhibit the oxidation of MXene and improve the structural stability due to its physical barrier and limited effect.

To investigate the reproducibility of the PEC sensor, the photocurrent values of five independently as-prepared $Ti_3C_2$ MXene/$Cd^{2+}$/FTO photo-electrode were measured for monitoring1.825 × $10^8$ particles per mL exosomes standard. The date indicated that the relative standard deviation (RSD) was calculated as 4.34%. As a proof of principle, the above results preliminarily proved the feasibility of PEC scheme and was expected to realize the practical application of exosomes.

Table 1 Recovery results of the spike-in experiment for exosome quantitation in 5% diluted supernatant of fetal bovine serum by the PEC biosensor

| Sample | Spike concentration (particles per mL) | Detected concentration (particles per mL) | Recovery (%) | RSD (%) |
|---|---|---|---|---|
| 1 | 7.3 × $10^6$ | 6.941 × $10^6$ | 95.08 | 2.05 |
| 2 | 7.3 × $10^7$ | 7.679 × $10^7$ | 105.19 | 1.69 |
| 3 | 1.752 × $10^8$ | 1.696 × $10^8$ | 96.80 | 3.85 |

### Biological sample testing

To explore the potential application of the proposed $Ti_3C_2$ MXene-anchored PEC biosensor, we simulated biological samples by injecting exosomes to 5% diluted supernatant of fetal bovine serum. As shown in Table 1, the photocurrent signal increased significantly with the increase of spiked exosomes concentration. The recoveries of exosomes were 95.08–105.19%, indicating that the accuracy of the proposed PEC biosensor for clinical sample testing was acceptable. These observations further demonstrated that our strategy might be of value for the detection of target exosomes in practical application.

## Conclusions

In summary, this work established the $Ti_3C_2$ MXene-anchored PEC biosensor based on the *in situ* synthesis of $Ti_3C_2$ MXenes/CdS composites by coupling with an enzyme-assisted amplification strategy for the quantitative detection of exosomes. Above all, magnetic separation technology and HCR strategy not only specifically enriched the target exosomes and simplified the operation, which was conducive to the construction of a universal and easy-to-operate platform, but also an amplification strategy to introduce more enzymes through DNA assembly. Such a strategy focused on enzyme-induced CdS deposition on $Ti_3C_2$ MXene to form $Ti_3C_2$ MXenes/CdS composites, which produced a built-in electric field in the tight interface between CdS and MXenes, and promoted the separation and migration of photo-generated carriers due to the matching energy level. Whereas, our method still has some shortcomings. But still, the proposed strategy remained some drawbacks. The individual detection steps were various and time-consuming, which limited its clinical application. Inspiringly, the testing process of this novel PEC biosensor didn't require the additional purification of samples, and obtained satisfactory performance, acceptable stability and reproducibility. As a consequence, our diagnostic approach could provide a viable option for sensitive detection of exosomes and expand to other clinical applications.

## Author contributions

Zhenli Qiu:investigation, design of methodology, supervision, writing – review & editing. Dechun Fan: formal analysis, writing-original draft. XiangHang Xue: investigation. Jiayi Zhang: investigation. Jiaolin Xu: investigation. HaixiaLyu: conceptualization, supervision. Yiting Chen: conceptualization, supervision, funding acquisition, writing – review & editing.

## Conflicts of interest

There are no conflicts to declare.

## Acknowledgements

Support by the National Natural Science Foundation of China (22004053), the National Science Foundation of Fujian Province (2021J05203, 2019J01757), Fuzhou science and technology project (Ecological City Construction and Social Development Comprehensive Project) (2020-S-30), and the Education research project of Young and middle-aged teachers in Fujian Province (JAT190603) is gratefully acknowledged.

## Notes and references

1 C. He, S. Zheng, Y. Luo and B. Wang, *Theranostics*, 2018, **8**, 237–255.
2 A. J. O'Loughlin, C. A. Woffindale and M. J. A. Wood, *Curr. Gene Ther.*, 2012, **12**, 262–274.
3 F. He, J. Wang, B. C. Yin and B. C. Ye, *Anal. Chem.*, 2018, **90**, 8072–8079.
4 M. Takasugi, R. Okada, A. Takahashi, D. V. Chen, S. Watanabe and E. Hara, *Nat. Commun.*, 2017, **8**, 15729.
5 S. A. Melo, L. B. Luecke, C. Kahlert, A. F. Fernandez, S. T. Gammon, J. Kaye, V. S. LeBleu, E. A. Mittendorf, J. Weitz, N. Rahbari, C. Reissfelder, C. Pilarsky, M. F. Fraga, D. Piwnica-Worms and R. Kalluri, *Nature*, 2015, **523**, 177–182.
6 Z. Wang, S. Zong, Y. Wang, N. Li, L. Li, J. Lu, Z. Wang, B. Chen and Y. Cui, *Nanoscale*, 2018, **10**, 9053–9062.
7 S. Wang, L. Zhang, S. Wan, S. Cansiz, C. Cui, Y. Liu, R. Cai, C. Hong, I. T. Teng, M. Shi, Y. Wu, Y. Dong and W. Tan, *ACS Nano*, 2017, **11**, 3943–3949.
8 H. Im, H. Shao, Y. I. Park, V. M. Peterson, C. M. Castro, R. Weissleder and H. Lee, *Nat. Biotechnol.*, 2014, **32**, 490–495.
9 C. Liu, X. Zeng, Z. An, Y. Yang, M. Eisenbaum, X. Gu, J. M. Jornet, G. K. Dy, M. E. Reid, Q. Gan and Y. Wu, *ACS Sens.*, 2018, **3**, 1471–1479.
10 W. Liu, J. Li, Y. Wu, S. Xing, Y. Lai and G. Zhang, *Biosens. Bioelectron.*, 2018, **102**, 204–210.
11 N. Zhang, L. Zhang, Y. F. Ruan, W. W. Zhao, J. J. Xu and H. Y. Chen, *Biosens. Bioelectron.*, 2017, **94**, 207–218.
12 W. W. Zhao, J. J. Xu and H. Y. Chen, *Chem. Rev.*, 2014, **114**, 7421–7441.
13 J. Shu and D. Tang, *Anal. Chem.*, 2020, **92**, 363–377.
14 C. Q. Zhao and S. N. Ding, *Coord. Chem. Rev.*, 2019, **391**, 1–14.
15 M. R. Lukatskaya, O. Mashtalir, C. E. Ren, Y. Dall'Agnese, P. Rozier, P. L. Taberna, M. Naguib, P. Simon, M. W. Barsoum and Y. Gogotsi, *Science*, 2013, **341**, 1502–1505.
16 M. Naguib, V. N. Mochalin, M. W. Barsoum and Y. Gogotsi, *Adv. Mater.*, 2014, **26**, 992–1005.
17 X. Zhu, Y. Zhang, M. Liu and Y. Liu, *Biosens. Bioelectron.*, 2021, **171**, 112730.
18 L. Ding, L. Li, Y. Liu, Y. Wu, Z. Lu, J. Deng, Y. Wei, J. Caro and H. Wang, *Nat. Sustainable*, 2020, **3**, 296–302.
19 X. Wu, Z. Wang, M. Yu, L. Xiu and J. Qiu, *Adv. Mater.*, 2017, **29**, 1607017.
20 L. Zhang, Z. Luo, R. Zeng, Q. Zhou and D. Tang, *Biosens. Bioelectron.*, 2019, **134**, 1–7.
21 Y. Xu, S. Wang, J. Yang, B. Han, R. Nie, J. Wang, J. Wang and H. Jing, *Nano Energy*, 2018, **51**, 442–450.

22 R. B. Rakhi, B. Ahmed, M. N. Hedhili, D. H. Anjum and H. N. Alshareef, *Chem. Mater.*, 2015, **27**, 5314–5323.
23 C. Peng, X. Yang, Y. Li, H. Yu, H. Wang and F. Peng, *ACS Appl. Mater. Interfaces*, 2016, **8**, 6051–6060.
24 M. Naguib, M. Kurtoglu, V. Presser, J. Lu, J. Niu, H. Min, L. Hultman, Y. Gogotsi and M. W. Barsoum, *Adv. Mater.*, 2011, **23**, 4207.
25 Y. Li, L. Ding, Y. Guo, Z. Liang, H. Cui and J. Tian, *ACS Appl. Mater. Interfaces*, 2019, **11**, 41440–41447.
26 X. Hu, S. Lu, J. Tian, N. Wei, X. Song, X. Wang and H. Cui, *Appl. Catal., B*, 2019, **241**, 329–337.
27 Z. Wu, H. Li and Z. Liu, *Sens. Actuators, B*, 2015, **206**, 531–537.
28 Z. Qiu, J. Shu and D. Tang, *Anal. Chem.*, 2017, **89**, 5152–5160.
29 H. Chen, F. Yuan, S. Wang, J. Xu, Y. Zhang and L. Wang, *Biosens. Bioelectron.*, 2013, **48**, 19–25.
30 K. Sumit, I. J. Michael, P. Juhee, G. Steve and Y. K. Cho, *Small*, 2018, **14**, 1870154.
31 D. I. Kim, M. A. Islam, L. Avila and I. P. Herman, *J. Phys. Chem. B*, 2003, **107**, 6318–6323.